



Article

# Flexural Fatigue Test—A Proposed Method to Characterize the Lifetime of Conductor Tracks on Polymeric Substrates

Simon Petillon <sup>1,2,\*</sup> , Andrea Knöller <sup>1</sup>, Philipp Bräuer <sup>3</sup>, David Helm <sup>1</sup>, Tobias Grözinger <sup>1</sup>, Sascha Weser <sup>1</sup>, Wolfgang Eberhardt <sup>1</sup>, Jörg Franke <sup>3</sup> and André Zimmermann <sup>1,2</sup>

<sup>1</sup> Hahn-Schickard, 70569 Stuttgart, Germany; andrea.knoeller@hahn-schickard.de (A.K.); david.helm@hahn-schickard.de (D.H.); tobias.groeziinger@hahn-schickard.de (T.G.); sascha.weser@hahn-schickard.de (S.W.); wolfgang.eberhardt@hahn-schickard.de (W.E.); andre.zimmermann@ifm.uni-stuttgart.de (A.Z.)

<sup>2</sup> Institute for Micro Integration (IFM), University of Stuttgart, 70569 Stuttgart, Germany

<sup>3</sup> Institute for Factory Automation and Production Systems (FAPS), Friedrich-Alexander University Erlangen-Nürnberg, 90429 Nürnberg, Germany; philipp.braeuer@faps.fau.de (P.B.); joerg.franke@faps.fau.de (J.F.)

\* Correspondence: simon.petillon@hahn-schickard.de; Tel.: +49-711-685-83772

**Abstract:** High quality and long product life are two fundamental requirements for all circuit carriers, including molded interconnect devices (MID), to find application in various fields, such as automotive, sensor technology, medical technology, and communication technology. When developing a MID for a certain application, not only the design, but also the choice of material as well as the process parameters need to be carefully considered. A well-established method to evaluate the lifetime of such MID, respective of their conductor tracks, is the thermal shock test, which induces thermomechanical stresses upon cycling. Even though this method has numerous advantages, one major disadvantage is its long testing time, which impedes rapid developments. Addressing this disadvantage, this study focuses on the laser direct structuring of thermoplastic LCP Vectra E840i LDS substrates and the subsequent electroless metallization of the commonly used layer system Cu/Ni/Au to force differences in the conductor tracks' structure and composition. Performing standardized thermal shock tests alongside with flexural fatigue tests, using a customized setup, allows comparison of both methods. Moreover, corresponding thermomechanical simulations provide a direct correlation. The flexural fatigue tests induce equivalent or even higher mechanical stresses at a much higher cycling rate, thus drastically shorten the testing time.

**Keywords:** conductor track; flexural fatigue test; laser direct structuring; metallization; molded interconnect device



**Citation:** Petillon, S.; Knöller, A.; Bräuer, P.; Helm, D.; Grözinger, T.; Weser, S.; Eberhardt, W.; Franke, J.; Zimmermann, A. Flexural Fatigue Test—A Proposed Method to Characterize the Lifetime of Conductor Tracks on Polymeric Substrates. *J. Manuf. Mater. Process.* **2022**, *6*, 41. <https://doi.org/10.3390/jmmp6020041>

Academic Editors: Antonio Riveiro and Rafael Comesaña

Received: 28 February 2022

Accepted: 29 March 2022

Published: 1 April 2022

**Publisher's Note:** MDPI stays neutral with regard to jurisdictional claims in published maps and institutional affiliations.



**Copyright:** © 2022 by the authors. Licensee MDPI, Basel, Switzerland. This article is an open access article distributed under the terms and conditions of the Creative Commons Attribution (CC BY) license (<https://creativecommons.org/licenses/by/4.0/>).

## 1. Introduction

Circuit carriers, such as conventional printed circuit boards (PCB) based on FR4, are the backbone of almost every electronic system. However, advances in individualization, miniaturization and functionalization triggered the demand for novel circuit carriers beyond 2D-boards. In the last two decades, especially laser direct structured molded interconnect devices (LDS-MID [1]), of which the fabrication process is schematically depicted in Figure 1a, aroused great interest due to their numerous advantages: (i) Fabricating 3D-substrates via injection molding of thermoplastic materials unlocks an unprecedented design freedom, which helps effectively utilize a given, restricted space. (ii) The presence of laser activatable additives in the thermoplastic materials enables the laser direct structuring (LDS), pioneered by LPKF [2], and allows subsequent electroless metallization of electrically conducting structures, thus drastically decreasing the number of fabrication steps as compared to conventional fabrication methods for PCB [3]. (iii) Moreover, these fully mask-less process steps boost the possibility of individualized circuits and enable fast

layout changes. (iv) Finally, mounting electronic components, such as resistors, sensors, chips, or light-emitting diodes, in a three-dimensional fashion increases the integration density, which is beneficial for the demand for miniaturization. These advantages enabled MID to break into the electronic market, already finding application in the fields of automotive, sensor technology, medical technology, and communication technology [1].

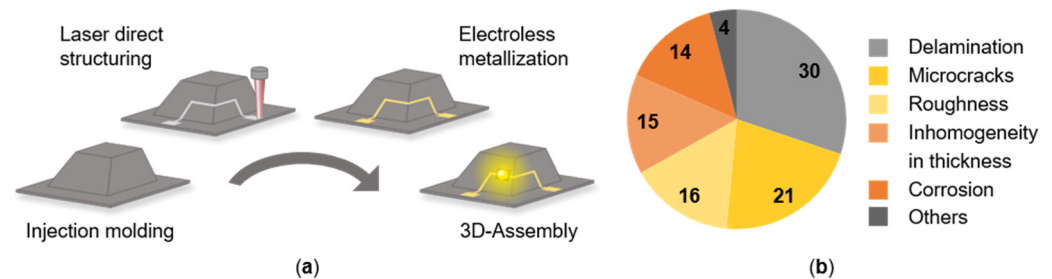


**Figure 1.** (a) Schematic depiction of the LDS-MID process chain; (b) Percentage of main causes of failure of conductor tracks on MID, according to Ref [4].

In order to further push the acceptance of MID as competitive circuit carriers and to broaden the possible fields of application, it is essential to address the challenges of the MID technology. One challenge is to identify and eliminate the origin of possible defects, which limit the performance and lifetime of the conductor tracks on MID. Along this line, representatives from industry were interviewed in a former study, agreeing on the metallization process to be one of the most critical fabrication steps [4]. In terms of the complete MID's performance, particular delamination due to poor adhesion between conductor track and substrate, as well as the occurrence of microcracks within the conductor tracks were identified as the main causes of failure, as displayed in Figure 1b. Such possible causes of failure can be detected when performing a thermal shock test, which induces thermomechanical stress within the conductor tracks due to differences in the thermal expansion of the polymeric substrate and the metallic conductor track. Monitoring the electrical resistance of the conductor tracks during cycling further allows the detection of the exact time of failure as well as temporary defects [5]. This type of test is well-established for investigating the lifetime of electronic parts due to several advantages, especially the possibility to measure many samples at once and the ability to investigate 3D geometries.

Even though the thermal shock test is a powerful tool for the development of high-performance MID, they are also time consuming, e.g., a standardized test (DIN EN ISO 60068) of 2000 cycles takes about 42 days. In order to shorten the development period, or if an in-process quality control is required, alternative test types need to be considered. One alternative is the flexural fatigue test, which is typically applied to investigate metals [6], concrete [7–10] or printed/flexible electronics [11–13]. As thermoplastic MID substrates likewise exhibit a certain degree of mechanical flexibility, the flexural fatigue test is a suitable candidate. In general, it can be distinguished between 2-, 3-, and 4-point flexural tests. While the 3-point flexural test might be the most common test setup, the 4-point flexural test allows eliminating shear in the zone between the two indenters, yielding a constant bending moment. This 4-point setup thus eliminates shear and leads to the most accurate results. However, the 4-point geometry is mostly suitable when considering the bulk material. In case of MID, the focus lies on the electrical performance of the conductor tracks on the polymeric substrate, which can be monitored via the change in electrical resistance during cycling. Here, the 4-point-geometry impedes the possible circuitry, as the conductor tracks need to have a sufficient electrical contact and cannot run in the area of the supporting points and the indenters. A direct contact between conductor track and the fixtures would mechanically stress the conductor track beyond the impact of bending upon cycling, compromising the results.

Therefore, in a previous study, a customized 2-point flexural setup, which was constructed based on a testing device found in reference [14], was used to identify influencing factors on the lifetime of conductor tracks on MID [15]. Although this method is limited to 2D geometries, it provides fundamental knowledge of the impact of different parameters, including laser-induced roughness, metal thickness, and metal composition, on the MID's performance in a much shorter period than with thermal shock tests. However, it also raises the question to what extent such a test is comparable to the standardized thermal shock test. Taking up this study, here we consciously vary the laser as well as metallization parameters to tailor the conductor tracks, forcing defined differences in microstructure and composition on the widely applicable substrate material LCP Vectra E840i LDS. Samples for thermal shock tests and flexural fatigue tests were processed together to ensure a direct comparison, when being tested. In addition, thermomechanical simulations were carried out to correlate the thermally induced strain of the conductor tracks with an equivalent mechanical deflection under flexural load. The aim was to investigate if the results of the flexural fatigue tests mirror the ones of the standard thermal shock tests, but on a much smaller time scale.

## 2. Materials and Methods

### 2.1. Sample Fabrication

All samples were fabricated according to the well-established process chain of the MID-technology [1]. Among the available LDS thermoplastics, LCP Vectra E840i LDS (LCP) from Celanese stands out due to its molecular structure composed of aligned liquid crystal polymers, which leads to a distinct mechanical stiffness along with a good thermal and chemical stability. These characteristics make it widely applicable. Moreover, it is known to form a distinct sponge-like surface structure upon LDS with a 1064 nm, diode-pumped Nd:YAG laser (LPKF MicroLine 3D 160i; 60  $\mu\text{m}$  spot size), as displayed in Figure 2a. This sponge-like structure could be tailored by the choice of laser parameters, specifically the laser power. A subsequent cleaning process could further modify it, e.g., using a low laser power, combined with a CO<sub>2</sub> snow jet cleaning resulted in mostly dense and smooth surfaces. The electroless metallization of such surfaces with Cu/Ni/Au yielded a roughness  $R_a$  of 1.2  $\mu\text{m}$  (Figure 2b), as measured by a standardized tactile profile measurement on specific conductor tracks [16]. Such low roughness is especially suitable if wire bonding is required for chip assembly, as tested with a Wire Bonder G5 Single of F&K Delvotec (inset of Figure 2c). However, a low roughness corresponded to a low adhesive strength of the metal layer (Figure 2c). The latter could be extracted from hot pin pull tests [17] with a Dage4000 on the circular structures displayed in Figure 2b. Therefore, suitable laser parameter sets needed to be carefully considered. For the current study, a laser power of 0.85 and 2 W as well as wet chemical cleaning were chosen to generate a significant difference in roughness (Table 1) without lacking in proper adhesive strength, according to Figure 2c.

Besides the above-mentioned laser parameters, different metallization parameters were also considered. In the previous study [15], the nickel layer was identified to be responsible for crack initiation upon flexural bending. Therefore, the copper- and gold plating in the given layer system Cu/Ni/Au was kept constant, while the nickel layer was varied in thickness and chemical composition. The thickness of the nickel layer was varied via the bath parameters, specifically the plating time. When aiming at compositional variations, different electrolytes needed to be used. In general, nickel layers, which are obtained from electroless plating, typically contain a certain amount of phosphorous. It can be distinguished between a low (2–5 wt.%; Low-Phos), a medium (6–9 wt.%; Mid-Phos), and a high phosphorous content (10–13 wt.%; High-Phos).

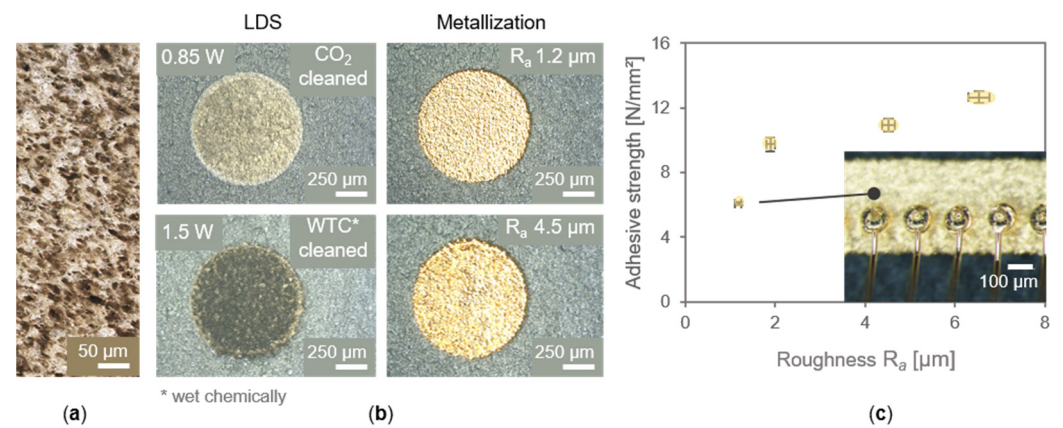


**Figure 2.** (a) Laser structured area of LCP, exhibiting a distinct sponge-like surface; (b) Surface after laser structuring with different laser power and cleaning processes and after metallization with Cu/Ni/Au; (c) Correlation of roughness and adhesive strength of the resulting metallization. The inset displays the possibility of wire bonding for the metallization with the lowest roughness.

**Table 1.** Structural and compositional features of conductor tracks for lifetime tests obtained from different laser \* and metallization \*\* parameters.

| Variant | Roughness $R_a$ ( $\mu\text{m}$ ) | Nickel Thickness ( $\mu\text{m}$ ) | Phosphorous Content in Nickel (wt.%) |
|---------|-----------------------------------|------------------------------------|--------------------------------------|
| V1      | 1.9                               | 0                                  | -                                    |
| V2      | 1.9                               | 5                                  | 6.4                                  |
| V3      | 1.9                               | 9                                  | 6.4                                  |
| V4      | 6.5                               | 5                                  | 6.4                                  |
| V5      | 6.5                               | 3                                  | 6.4                                  |
| V6      | 6.5                               | 3                                  | 12.0                                 |

\* Laser power 0.85 W vs. 2 W. Laser frequency and scan speed were kept constant at 100 Hz and 1000 mm/s, respectively. All samples underwent a wet chemical cleaning before metallization. \*\* Variation of plating time between 10 and 22 min to obtain different nickel thicknesses. Cu400SC copper plating (~8  $\mu\text{m}$  thickness) and Aurol 20 gold plating (~0.1  $\mu\text{m}$  thickness) were kept constant for all samples.

Depending on the phosphorous content, the nickel layers exhibit different properties [18]. For example, the density linearly decreases with the phosphorous content, while the electrical resistance shows an opposing trend. Aiming at improving the mechanical performance to enhance the lifetime of conductor tracks on MID, the ductility and the internal stresses of the nickel layers are the most important parameters to consider, as displayed in Figure 3a. The ductility of the nickel layer reaches its minimum at a phosphorous content of 8 wt.% (Mid-Phos). Simultaneously, the internal stresses reach their maximum of 40 MN/m<sup>2</sup>. Therefore, Mid-Phos nickel layers are less ductile and are constantly under tensile stress, making them prone to mechanical failure, as depicted in Figure 3b, top. Despite these facts, Mid-Phos electroless nickel electrolytes (here Durnicoat 520) are widely applied in electronics manufacturing and were also used for the fabrication of most of the here used samples (Table 1). Energy dispersive X-ray spectroscopy (EDX) investigations revealed an average phosphorous content of 6.4 wt.% (Figure 3a, orange line) for these samples. In contrast, High-Phos nickel electrolytes result in more ductile nickel layers, which are under compressive tension, making them mechanically more resilient. Fabricating samples with an High-Phos nickel electrolyte (Nimuden 858-AF), resulted in nickel layers with an average phosphorous content of 12 wt.% (yellow line), likewise obtained by EDX (Table 1).

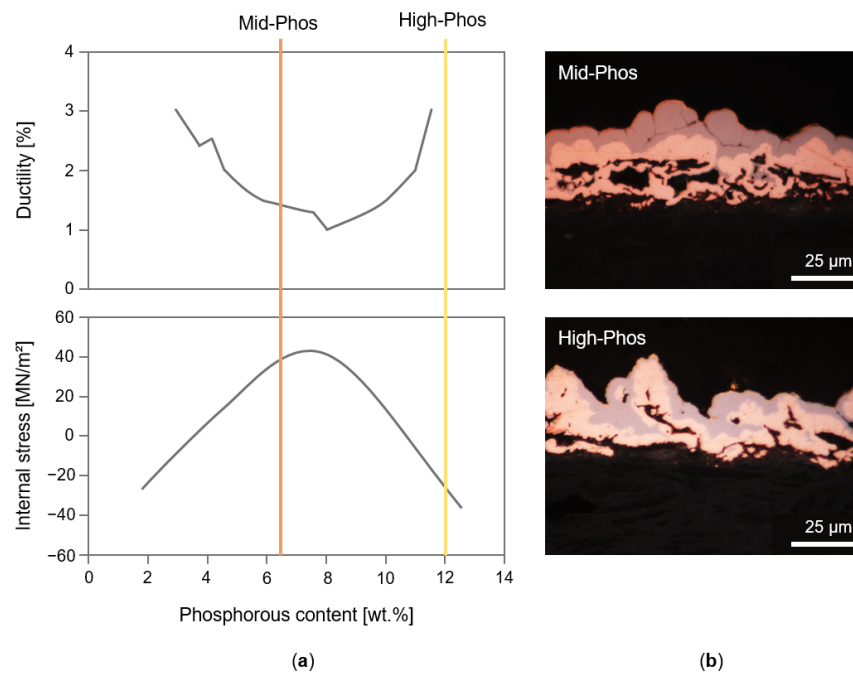


**Figure 3.** (a) Influence of the phosphorous content in electroless nickel on the ductility and internal stresses of the resulting metal layer, as adapted from Ref. [18]. The orange and yellow highlighted phosphorous contents, determined by EDX, were applied in this study; (b) Cross-section images of Cu/Ni/Au conductor tracks revealing cracks in the Mid-Phos nickel layer.

In order to fabricate samples of the listed variants, the LCP was injection-molded according to the specification sheet of [19], using an Arburg 370 A. Two different geometries were discharged, a plaque ( $3.7 \times 3.7 \text{ cm}^2$ ) suitable for the thermal shock test and a bone-shaped geometry (7.9 cm in length) suitable for the flexural fatigue tests. Layouts for both geometries were defined, which were used for actually processing samples for both type of tests, as displayed in Figure 4, as well as for thermomechanical simulations.

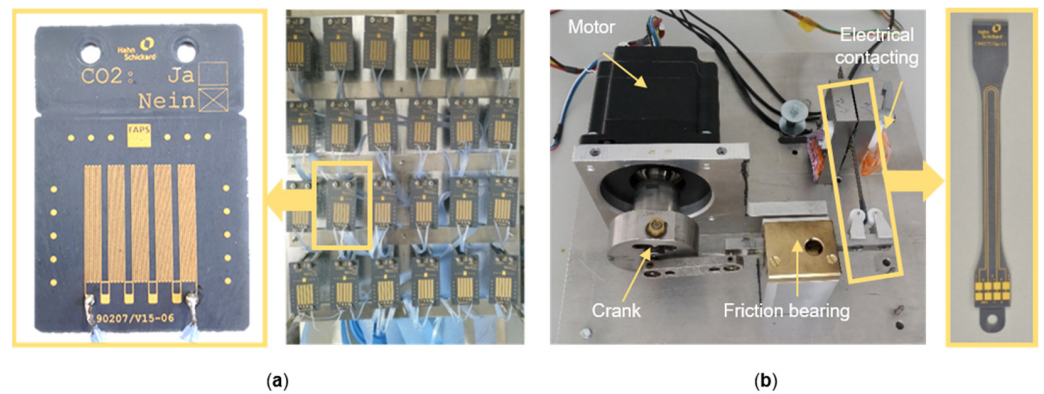


**Figure 4.** (a) Setup for thermal shock tests and the corresponding sample; (b) Customized setup for flexural fatigue tests and the corresponding sample.

## 2.2. Lifetime Investigations

Standard thermal shock tests were carried out in a Vötsch VT3 7012 P2 according to DIN EN ISO 60068, in which the samples were being rapidly transferred from one chamber ( $-40 \text{ }^\circ\text{C}$ ) to the other chamber ( $+140 \text{ }^\circ\text{C}$ ). The dwell time was 15 min in each chamber, summing up to a total cycle time of 30 min. Testing 2000 cycles to obtain robust data required 1000 h ( $\sim 42$  days). During that period, the electrical resistance of the conductor

tracks was monitored. Reaching a certain threshold value, here greater than 20% increase, marked the maximum number of cycles before failure.

While the thermal shock tests were standardized, the customized flexural fatigue test setup required initial investigations in terms of frequency and deflection (Figure 5). It appeared that higher frequencies and larger deflections significantly heated the samples. While different deflections needed to be investigated to obtain a Woehler plot, also known as an S-N curve, only the lowest frequency was used for all following flexural fatigue tests to minimize the thermal impact during measurements. Operating at 25 Hz allowed measuring 25 cycles per second, thus 2000 cycles in 80 s. The customized setup enabled repeated bending of bone-shaped 2D substrates in both directions, whereas the deflection could be varied, ranging from 5 to 12 mm in both directions, so that the conductor tracks were stretched and compressed in an alternating fashion (Figure 4b). The substrates were featured with two conductor tracks per side, allowing simultaneous conduction of four measurements. During cycling, the mechanical failure of the conductor tracks was monitored with the help of an event detector. In case of mechanical failure, which was represented by cracks propagating perpendicular to the conductor track's orientation, the electrical resistance exceeded the pre-defined threshold value of 60  $\Omega$ , marking the maximum number of cycles.

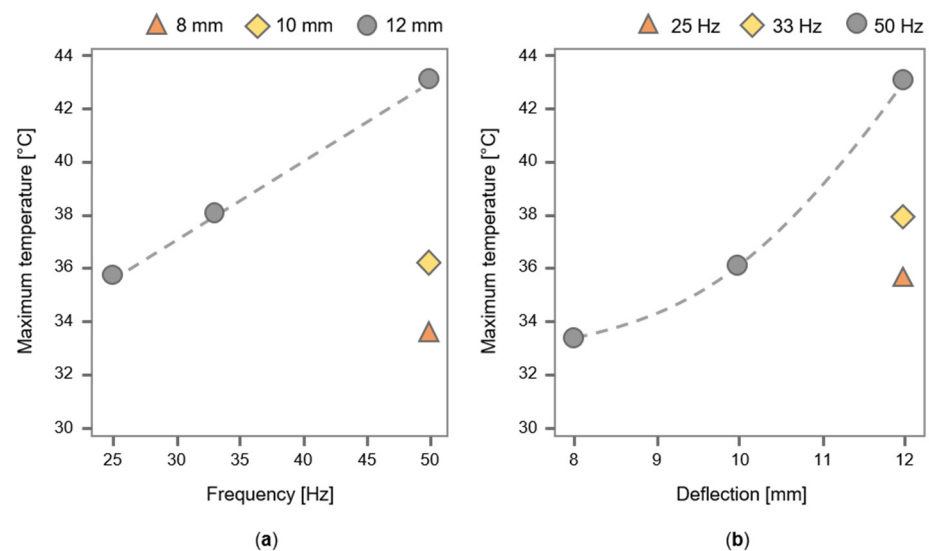


**Figure 5.** Initial flexural fatigue tests to investigate the influence of (a) frequency on the maximum temperature for different deflections and (b) deflection on the maximum temperature for different frequencies.

For each deflection, at least 12 identical conductor tracks were investigated. The analysis was carried out using Minitab, which allowed the identification of outlier via box plots, the determination of significance via t-test, as well as the determination of the average lifetime. For each type of measured sample, at least three different deflections were considered to construct a Woehler plot. Such plot allows extrapolating the maximum number of cycles for further deflections. It has to be noted that, unlike the classical Woehler plot, the diagrams presented here do not display the stress. The strongly irregular geometry of the conductor tracks obtained by the LDS process, as visualized in Figure 3b, impeded the calculation of the stress, which was induced in the conductor track upon flexural load. Alternatively, the maximum deflection of the sample was used. Coherent with the induced stresses, the larger the deflection, the less cycles a sample could bear before failure.

### 2.3. Thermomechanical Simulation

The simulations were performed using the FEM tool Ansys Workbench. The geometry of the substrates and the conductor tracks was taken into account in the simulation models

so that both variants, shown in Figure 6, could be compared. The Cu/Ni conductor tracks were modeled with a total thickness of 10 μm. The used materials' data, Young's modulus, and coefficient of thermal expansion (CTE) is shown in Table 2.

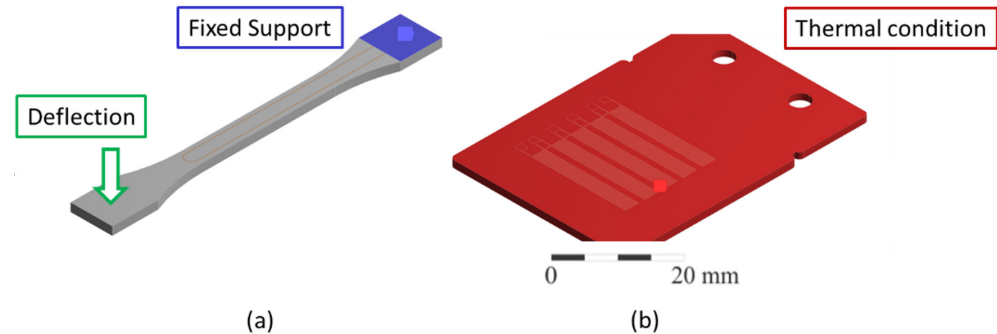


Figure 6. Boundary conditions of simulation for (a) flexural fatigue test and (b) thermal shock test.

Table 2. Materials' data, on which the simulations are based [20].

| Material | Young's Modulus <sub>20°C</sub> [GPa] | Young's Modulus <sub>20°C</sub> †[GPa] | CTE <sub>-40°C</sub> [ppm/K] †/‡ | CTE <sub>150°C</sub> [ppm/K] †/‡ |
|----------|---------------------------------------|--|----------------------------------|----------------------------------|
| LCP      | 10.3                                  | 6.0                                    | 9.2/23.2                         | 14.3/32.7                        |
| Cu/Ni    | 99.8                                  |  | 15.4                             | 15.4                             |

Figure 6 shows the boundary conditions for the simulation of (a) the bending fatigue test and (b) the thermal shock test. In the simulation of the bending test, the specimen was mechanically fixed at one end (blue) and deflected between 1 mm and 6 mm at the other end (green arrow), in accordance with the mountings on the test rig. For the simulative estimation of the strains in the thermal shock test, the entire assembly was thermally loaded to 125 °C and 150 °C. The reference temperature of the stress-free state was assumed to be at 20 °C.

### 3. Results

#### 3.1. Flexural Fatigue Tests

Performing flexural fatigue tests on samples with a different roughness revealed a significant increase in number of cycles before failure for all three investigated deflections. The maximum number of cycles was up to two orders of magnitude larger for samples with a higher roughness (Figure 7a). Subsequent microstructural investigations of the samples cross-section depicted the origin of the superior mechanical lifetime of these samples (Figure 7b).

Closer inspection revealed that the interlocked layer between substrate and metal layer was much more pronounced for samples with an increased roughness, generated by a higher laser power. Once a crack formed, the crack needed to propagate through an effectively thicker copper zone due to the additional interlocking layer. Moreover, the interpenetrated network of polymer and metal promoted crack deflection, which is also a toughening mechanism widespread in nature. One of the most prominent biological examples is nacre, which is composed of inorganic platelets embedded into a biopolymer matrix [21]. This so-called brick-and-mortar microstructure exhibits an extra-ordinary combination of strength (due to the interlocking of the components) and toughness (due to the crack deflection around the inorganic platelets). Both properties are also essential for the design of high-performance MID, considering the main causes of failure (Figure 1b).

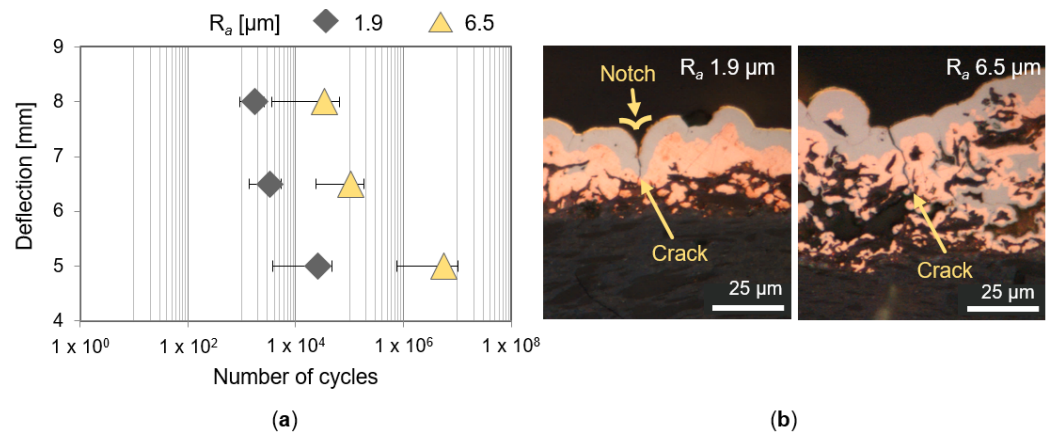


**Figure 7.** (a) Number of cycles dependent on the deflection and the roughness  $R_a$ , whereas the nickel thickness was 5  $\mu\text{m}$ ; (b) Cross-section image of conductor tracks after mechanical failure.

The investigation of the conductor tracks' cross-section after failure further confirmed that cracks form preferably in the center of a notch (Figure 7b) in the nickel layer. Upon repeated flexural load, the crack propagated into the copper layer until total failure. Therefore, samples with Cu/Ni/Au layers having different nickel layer thickness as well as samples with pure copper layers were being mechanically tested. The corresponding Woehler plots in Figure 8a display the impact of the nickel thickness on the number of cycles. Decreasing the nickel thickness from 9  $\mu\text{m}$  to 5  $\mu\text{m}$  increased the maximum number of cycles by up to one order of magnitude. This result verified that the nickel layer is responsible for the crack formation and correlated well with the findings of [22], where it is stated that nickel appears to be more brittle than copper and an increase in layer thickness likewise increases the stiffness of the layers. The maximum number of cycles could be further enhanced when no nickel is plated onto the copper layer. However, in the well-established metal layer system Cu/Ni/Au, which is used for PCB as well as for MID, the nickel serves as a diffusion barrier between the electrically conducting copper and the gold finish. The latter prevents corrosion and enables different assembly technologies, including soldering. Therefore, totally abstaining from nickel was not an option, but decreasing the nickel thickness was beneficial for the lifetime of the conductor tracks. It was important to find a trade-off between layers thick enough to ensure the diffusion barrier and thin enough to minimize the risk of crack formation. Thus, the nickel thickness was set to 3  $\mu\text{m}$ , along with a  $R_a$  of 6.5  $\mu\text{m}$ , for the samples with different phosphorous content in the nickel.

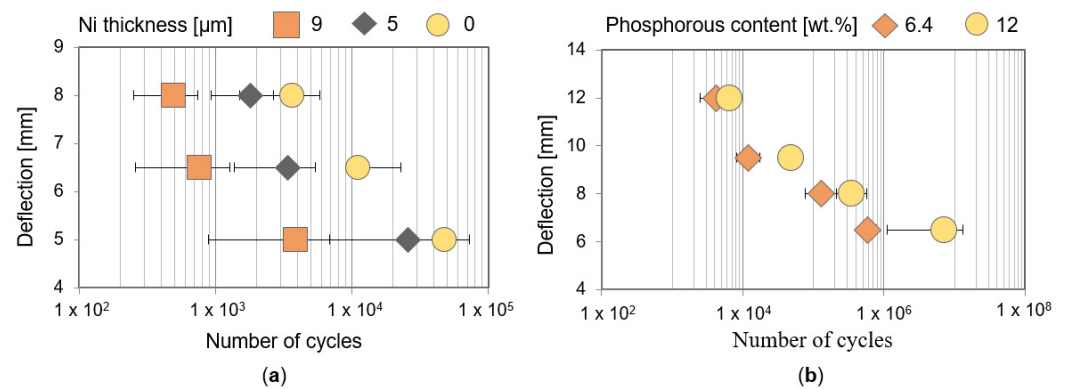


**Figure 8.** Number of cycles dependent on the deflection and (a) the thickness of the nickel layer, whereas the roughness  $R_a$  was 1.9  $\mu\text{m}$ ; (b) the phosphorous content in the nickel layer, whereas the roughness  $R_a$  was 6.5  $\mu\text{m}$  and nickel thickness was 3  $\mu\text{m}$ .

Another way to minimize the crack formation in the nickel layer was by varying the nickel electrolyte for plating. The corresponding Woehler plots are displayed in Figure 8b. For all tested deflections, the samples, prepared with the High-Phos nickel electrolyte, showed a superior mechanical stability. This superiority was more pronounced (one order of magnitude) for lower deflections, proving the mechanical advantage of using such electrolytes for the design of conductor tracks on MID with enhanced lifetime. For the largest tested deflection (12 mm), however, no significant difference in the maximum number of cycles could be detected. This finding implied that for severe flexural loads, the more ductile High-Phos nickel also reached a limit in mechanical performance.

### 3.2. Simulation-Assisted Correlation with Standardized Thermal Shock Tests

Thermomechanical simulations were carried out to correlate the mechanical deflection of the bone-shaped samples under flexural load (Figure 9a) with an equivalent, thermally induced strain of plate-like samples, during heating (Figure 9b), using the materials' data listed in Table 2. The simulation resulted in the correlation displayed in Figure 10. Considering LCP with its CTE values, heating to, e.g., 150 °C induced a thermal strain of 0.00215 mm/mm, which was equivalent to a mechanical deflection of 3.3 mm, thus close to the chosen minimum deflection of 5 mm in the conducted flexural fatigue tests.

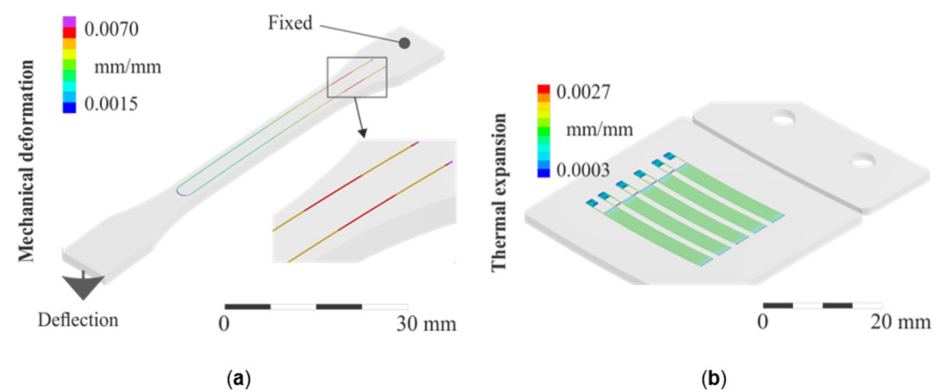


**Figure 9.** Simulation of the equivalent strain (a) during mechanical deformation and (b) during heating.

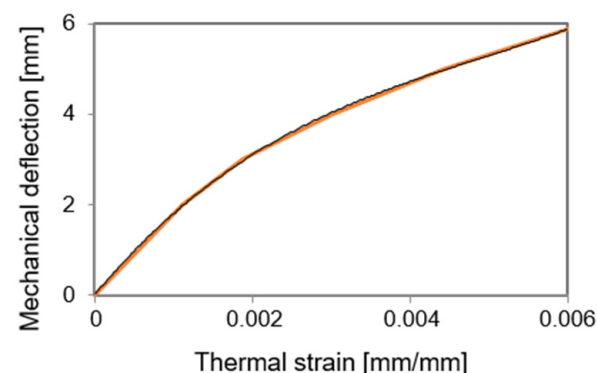


**Figure 10.** Correlation between mechanical deformation and thermal expansion as result of the conducted simulations.

In order to verify this correlation, standardized thermal shock tests (DIN EN ISO 60068) were carried out. Evaluating the data showed that an increased roughness and a decreased nickel layer thickness resulted in an increased number of thermal shock cycles, until reaching the threshold value of electrical resistance (Figure 11a). The mean time of failure was below 2000 cycles for these samples. Moreover, the roughness appeared to have the significantly larger effect on the lifetime.

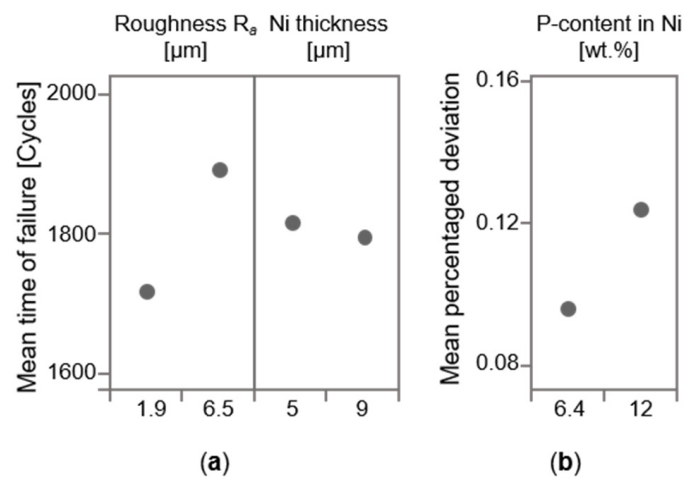


**Figure 11.** (a) Main and (b) minor influences extracted from thermal shock tests on samples prepared with the same laser and metallization parameters as for the flexural fatigue tests, but with the conductor track layout, which is displayed in Figure 4a.

After optimizing the roughness  $R_a$  (6.5  $\mu\text{m}$ ) and nickel thickness (3  $\mu\text{m}$ ), all samples fabricated with Mid-Phos as well as with High-Phos nickel endured the 2000 cycles without exceeding the threshold value. Closer inspection of these samples showed that the increase in electrical resistance was slightly less for the samples containing Mid-Phos nickel (Figure 11b). A clear trend could not be detected.

#### 4. Discussion

One significant difference was the absolute number of cycles in both types of methods. While the thermal shock test was limited to 2000 cycles (~42 days) in this study, samples of the flexural fatigue test underwent up to 7,174,400 cycles. Considering a frequency of 25 Hz, this number of bending cycles sums up to only ~3.3 days, thus about 3500 times as many cycles in only 8% of the time. Nevertheless, comparing the results of the thermal shock tests with the results of the flexural fatigue tests revealed similar trends in lifetime, when it comes to design variations of the conductor tracks on LCP substrates. Moreover, the phosphorous content variation of the nickel layer appeared to have a larger impact on the mechanical stability (under flexural load) than on the thermomechanical stability.

These findings are a first promising step towards a direct correlation of thermal shock test and the much faster flexural fatigue test. However, certain advances still need to be made by improving the customized setup and the corresponding software. To date, two critical discrepancies in both methods are the impact of the temperature on the interaction between substrate and conductor track and the definition of the threshold value. During thermal shock test, not only does the thermal expansion cause the failure of the conductor track, but so too does the materials' properties, e.g., Young's modulus and CTE, and their interaction change upon a change in temperature. However, the flexural fatigue test was conducted at room temperature, not providing information regarding the influence of the latter factor.

Concerning the threshold value, the thermal shock test was set to standard 20% of the initial electrical resistance, which was monitored during the test. In contrast, the used flexural fatigue test setup allowed only to define an absolute threshold value, which triggered an event detector. This threshold value was extracted from an initial online measurement, as depicted in Figure 12. It shows that the electrical resistance steadily increased with time, respective to cycles. However, once a crack was formed and the conductor track was pulvinated, the electrical resistance was exhibiting a peak value. As soon as the sample bent in the opposite direction, the conductor track was dished. The compressive stress then temporarily closed the crack, resulting in a drop in electrical resistance. In the presented online measurement, the peak indicated the complete failure of

the conductor track, defining a threshold value of  $60 \Omega$  (orange line). This value was kept constant, independent of the initial resistance of the conductor tracks.

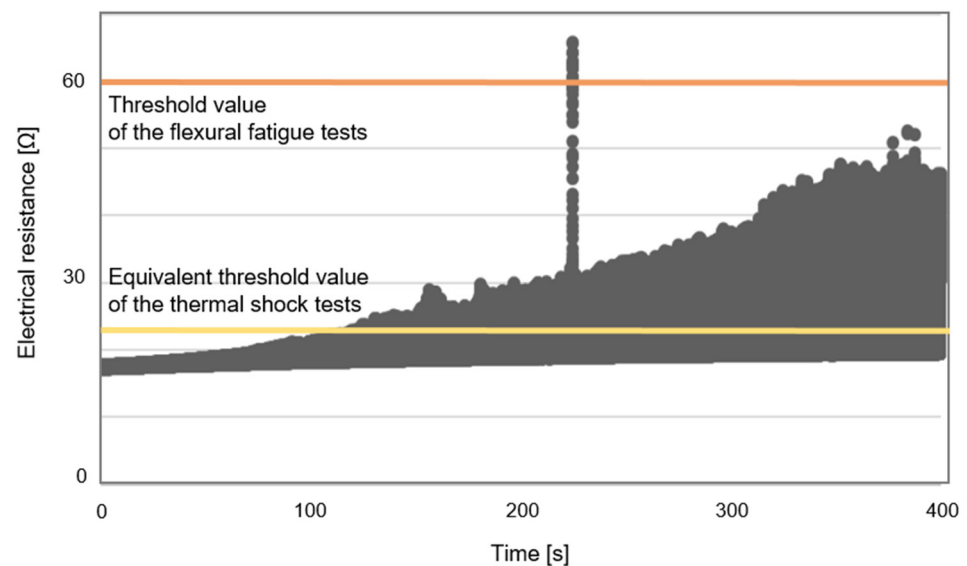


**Figure 12.** Determination of the threshold value for the flexural fatigue tests.

In order to resemble the criteria of failure used in the thermal shock tests, flexural fatigue tests should also be conducted at elevated temperatures and an equivalent threshold value needs to be defined for future investigations. Therefore, efforts will be made to upgrade the customized flexural fatigue test setup, so that it can be installed in a climatic chamber, and the corresponding software, so that it allows the monitoring of the electrical resistance and definition of a threshold value analog to the one of the standardized thermal shock test. In the example of Figure 12, when likewise using 20% of the initial value (yellow line), the threshold will be reached at a significant earlier point. This increases the sensitivity of the measurement and allows a closer correlation of the two test methods. Even though further advances can be made, the flexural fatigue test can never fully replace the thermal shock test, due to geometrical restrictions. However, it could be beneficial for a rapid assessment of process parameters, such as laser- and metallization parameters, which can be optimized in a 2D-setting. Thus, this method promotes an accelerated development of MID or if an in-process quality control is required.

## 5. Conclusions

The presented study can be condensed into four relevant conclusions:

- It could be verified that a high surface roughness and a low nickel thickness, along with an increased phosphorous content in the nickel layer, yields conductor tracks with an enhanced lifetime under flexural load.
- Similar trends regarding the lifetime of conductor tracks on MID were observed in comparison to a standardized thermal shock test, whereas the proposed method required a significantly shorter test time.
- Further adjustments of the flexural fatigue test setup need to be made to be able to also consider the influence of temperature on the polymer-metal bond in the proposed method as well as a comparable threshold value based on the initial resistance of each part, as in the case of the standardized thermal shock test.
- The flexural fatigue test cannot fully replace the standardized thermal shock test, as it is limited to 2D, but it can function as time-efficient supplementation, when compiling suitable process parameters for a certain application.

**Author Contributions:** Conceptualization, A.K. and P.B.; methodology, S.P., A.K., P.B. and T.G.; investigation, S.P., D.H., S.W., T.G. and P.B.; writing—original draft preparation, S.P. and A.K.; writing—review and editing, T.G., P.B. and W.E.; visualization, S.P. and A.K.; supervision, A.K. and W.E.; and funding acquisition, J.F. and A.Z. All authors have read and agreed to the published version of the manuscript.

**Funding:** This research was funded by the AiF, IGF-grant number 19754 N, which is funded by the Federal Ministry for Economic Affairs and Climate Action based on a resolution of the German Bundestag, as well as by the Deutsche Forschungsgemeinschaft (DFG), grant number 386746281.

**Data Availability Statement:** All data used are shown in the text. Raw data are available on request.

**Acknowledgments:** The authors thank Stephan Häusler and Katharina Strobel for the sample fabrication, as well as Johannes Kunz, Elisabeth Flechtner, Anke Bruha, and Ernst Müller for the sample characterization.

**Conflicts of Interest:** The authors declare no conflict of interest.

## References

1. Franke, J. *Three-Dimensional Molded Interconnect Devices (3D-MID): Materials, Manufacturing, Assembly and Applications for Injection Molded Circuit Carriers*; Carl Hanser Verlag GmbH & Co. KG: Munich, Germany, 2014; ISBN 978-1-56990-552-4.
2. Naundorf, G.; Wissbrock, H. Conductor Track Structures and Method for Production Thereof. U.S. Patent 7060421B2, 13 June 2006.
3. Khandpur, R.S. *Printed Circuit Boards: Design, Fabrication, Assembly and Testing*; Tata McGraw-Hill Education: New York, NY, USA, 2005; ISBN 978-0-07-058814-1.
4. Fechtelpeter, C.; Jürgenhake, C.; Fritz, K.-P.; Grözinger, T.; Müller, H.; Wild, P. *Zuverlässigkeit bei MID—Hemmnisse, Potentiale, Handlungsfelder (Reliability of MID—Obstacles, Potentials and Fields of Action)*; Forschungsvereinigung Räumliche Elektronische Baugruppen 3-D MID e.V.: Nuremberg, Germany, 2015.
5. Kuhn, T.; Franke, J. Influences on Crack Initiation in Conductor Tracks on Three-Dimensional Thermoplastic Substrates. In Proceedings of the 2017 Pan Pacific Microelectronics Symposium (Pan Pacific), Kauai, HI, USA, 6–9 February 2017; pp. 1–7.
6. Suárez, A.; Veiga, F.; de Lacalle, L.N.L.; Polvorosa, R.; Lutze, S.; Wretland, A. Effects of Ultrasonics-Assisted Face Milling on Surface Integrity and Fatigue Life of Ni-Alloy 718. *J. Mater. Eng. Perform.* **2016**, *25*, 5076–5086. [[CrossRef](#)]
7. AlShareedah, O.; Nassiri, S.; Dolan, J.D. Pervious Concrete under Flexural Fatigue Loading: Performance Evaluation and Model Development. *Constr. Build. Mater.* **2019**, *207*, 17–27. [[CrossRef](#)]
8. Kasu, S.R.; Deb, S.; Mitra, N.; Muppireddy, A.R.; Kusam, S.R. Influence of Aggregate Size on Flexural Fatigue Response of Concrete. *Constr. Build. Mater.* **2019**, *229*, 116922. [[CrossRef](#)]
9. Jia, Y.; Yang, Y.; Liu, G.; Gao, Y.; Yang, T.; Hu, D. Reliability Assessment of Flexural Fatigue Failure of Asphalt Mixture: A New Perspective. *Constr. Build. Mater.* **2020**, *257*, 119553. [[CrossRef](#)]
10. Carlesso, D.M.; Cavalaro, S.; de la Fuente, A. Flexural Fatigue of Pre-Cracked Plastic Fibre Reinforced Concrete: Experimental Study and Numerical Modeling. *Cem. Concr. Compos.* **2021**, *115*, 103850. [[CrossRef](#)]
11. Lall, P.; Narangaparantbil, J.; Leever, B.; Miller, S. Effect of Use Parameters on Fatigue-Life of Flexible Substrates under Bending Loads. In Proceedings of the 2019 18th IEEE Intersociety Conference on Thermal and Thermomechanical Phenomena in Electronic Systems (ITherm), Las Vegas, NV, USA, 28–31 May 2019; pp. 1072–1081.
12. Urasinska-Wojcik, B.; Chilton, N.; Todd, P.; Elsworth, C.; Bates, M.; Roberts, G.; Gibbons, G.J. Integrated Manufacture of Polymer and Conductive Tracks for Real-World Applications. *Addit. Manuf.* **2019**, *29*, 100777. [[CrossRef](#)]
13. Zhang, B.; Shan, G.; Su, F. Impact Reliability Analysis of a Rigid-Flex PCB System under Acceleration Loads. *Microelectron. Reliab.* **2021**, *127*, 114374. [[CrossRef](#)]
14. Grellmann, W.; Seidler, S. *Kunststoffprüfung*; Carl Hanser Verlag GmbH & Co. KG: Munich, Germany, 2015; ISBN 978-3-446-44390-7.
15. Mueller, H.; Groezinger, T.; Weser, S.; Eberhardt, W.; Zimmermann, A. Investigations on Flexural Fatigue Strength of Conductor Paths Fabricated by LPKF-LDS<sup>®</sup> Technology. *J. Micro Nano-Manuf.* **2017**, *6*, 011004. [[CrossRef](#)]
16. *DIN EN ISO 4288:1998-04*; Geometrical Product Specifications (GPS)—Surface Texture: Profile Method—Rules and Procedures for the Assessment of Surface Texture (ISO 4288:1996). Beuth Verlag GmbH: Berlin, Germany, 1998.
17. Goth, C.; Kuhn, T.; Gion, G.; Franke, J. Hot Pin Pull Method—New Test Procedure for the Adhesion Measurement for 3D-MID. Available online: <https://www.scientific.net/AMR.1038.115> (accessed on 28 December 2020).
18. Parkinson, R. *Properties and Applications of Electroless Nickel*; Nickel Development Institute: Toronto, ON, Canada, 1997.
19. VECTRA<sup>®</sup> E840i LDS. Available online: <https://tools.celanese.com/products/datasheet/US/VECTRA%C2%AE%20E840i%20LDS> (accessed on 21 February 2022).
20. Grözinger, T. Untersuchungen Zu Zuverlässigkeit Und Lebensdauermodellen Für Gelötete SMD Auf Spritzgegossenen Schaltungsträgern (Investigations of the Reliability and Life Cycle Models of Soldered SMD on Injection-Molded Circuit Carriers). Ph.D. Thesis, University of Stuttgart, Stuttgart, Germany, 2015.

21. Kakisawa, H.; Sumitomo, T. The Toughening Mechanism of Nacre and Structural Materials Inspired by Nacre. *Sci. Technol. Adv. Mater.* **2011**, *12*, 064710. [[CrossRef](#)] [[PubMed](#)]
22. Warkentin, D. Untersuchungen Zu Kapazitiven Beschleunigungssensoren Aus Metallbeschichtetem Kunststoff (Investigations on Capacitive Acceleration Sensors Made of Metal-Coated Plastic). Ph.D. Thesis, University of Stuttgart, Stuttgart, Germany, 2005.